



# Graphene-based tunable short band absorber for infrared wavelength

Vishal Sorathiya<sup>1</sup> · Sunil Lavadiya<sup>1</sup> · Leena Thomas<sup>2</sup> · Mohammed Abd-Elnaby<sup>3</sup> · Ahmed Nabih Zaki Rashed<sup>4</sup> · Mahmoud M. A. Eid<sup>5</sup>

Received: 29 April 2021 / Accepted: 20 December 2021 / Published online: 5 February 2022  
© The Author(s), under exclusive licence to Springer-Verlag GmbH Germany, part of Springer Nature 2022

## Abstract

The tunable graphene-based short band absorber has been numerically examined in this article. The absorption response of the proposed design has been analyzed with the variations of chemical potential, the radius of the resonator, width of the resonator, height of silver (Ag) resonator and the height of silica substrate. The proposed structure provides narrow band absorption and wideband response over an infrared wavelength of 1.5–1.6  $\mu\text{m}$ . It has been reported that absorption amplitude was up to 99%. Metamaterial behavior was analyzed by the calculation of permittivity, permeability and refractive index. We have also investigated the absorption and reflectance response of  $2 \times 2$  and  $3 \times 3$  array-based structures. Comparative analysis with the previously published article is also represented. Thanks to its tunability, efficiency, and self-alignment, the proposed absorber can find application as a compact high-contrast filter in infrared optical systems. This research work can also apply to the different research filed of designing sensors, polarisers, modulators, and many more.

## 1 Introduction

The research in the metamaterials field has grown extremely wide in a short period. It was back in the year 1898, an introduction of artificial materials for microwave applications was experimented with by Jagadis Chunder Bose which is now commonly known as chiral characteristics [1]. Since then there was a wide range of experiments performed like in the year 1914–1948 [2, 3], scientists procured a wide dimension of study regarding customizing the external properties of the material by fabricating artificially structures of various shapes and sizes. This new aspect of changing properties or creating material with non-existing properties generated a wide range of research into the field of metamaterials. It

offers some unrealistic exotic properties like negative permeability and permittivity [4]. Also, properties like negative refraction [5–7] perfect lensing [8] or superlens [9], and invisibility cloaking [10–12] are also created with the help of this kind of material.

On the contrary, another material which is researched widely in recent years is a 2D lattice structure named graphene [13]. Despite being monolayered, it outcastes some of the unique properties like flexibility, optical transparency [14], conductivity [15], and high electron mobility [16]. Also, ultra-wideband tunability can be achieved through an electrostatic field, magnetic field, or chemical doping by graphene [17, 18]. It depends on the different values such

✉ Ahmed Nabih Zaki Rashed  
ahmed\_733@yahoo.com  
Vishal Sorathiya  
vishal.sorathiya9@gmail.com  
Sunil Lavadiya  
splavadiya@gmail.com  
Leena Thomas  
leenathomas16@gmail.com  
Mohammed Abd-Elnaby  
maahmed@tu.edu.sa  
Mahmoud M. A. Eid  
m.elfateh@tu.edu.sa

<sup>1</sup> Department of Information and Communication Technology, Marwadi University, Rajkot 360003, Gujarat, India

<sup>2</sup> Department of Electronics and Communication Engineering, Marwadi Education Foundation's Group of Institutions, Rajkot 360003, Gujarat, India

<sup>3</sup> Department of Computer Engineering, College of Computers and Information Technology, Taif University, P.O. Box 11099, Taif 21944, Saudi Arabia

<sup>4</sup> Electronics and Electrical Communications Engineering Department, Faculty of Electronic Engineering, Menoufia University, Menouf 32951, Egypt

<sup>5</sup> Department of Electrical Engineering, College of Engineering, Taif University, P.O. Box 11099, Taif 21944, Saudi Arabia

as scattering rate, wavelength, and temperature based on the numerical study [19]. Owing to these aspects of graphene, it leads to one of the emerging possible platforms using electrically controlled nano-plasmonic for new-generation devices. Thus, graphene outsets a wide opportunity to achieve frequency tuning for metamaterial absorbers.

Owing to their properties, metamaterial- graphene-based perfect absorbers are the most research domain for the past few years. A significant amount of exertion has been intensive for achieving reduction in the loss in devices by developing numerous structural geometries. Recent researchers have observed strong circular dichroism effects in the region of near-infrared using summing up graphene layers strongly helping in the fields of optoelectronic devices and biosensing applications [20]. Based on the literature survey different shapes of tunable metamaterial absorber (MMA) is designed for near-infrared (NIR) wavelength between 1200 and 1600 nm to show the maximum absorption. A plasmon-induced tunable metasurface is engineered to have an overall linear absorption [21]. A multi-band tunable absorber coupled with a structured nanostructured material is proposed in [22] for sensing applications at wavelengths of about 800–1000 nm, which can be applied for manufacturing high sensitivity sensors. A triple-band MMA with an Au nanocuboids array is investigated in [23] and observed to have a triple-band tunable perfect absorption peak in the NIR band. In [24], a NIR Fano resonance in a hybrid metal-graphene metamaterial is clarified, where it has high-performance in the mid-infrared region with 0.93  $\mu\text{m}/\text{RIU}$  for sensitivity and about 158.7 for figure of merit (FOM). A circular and elliptical series of patterned graphene resonators on a silicon substrate with a silicon dioxide insulating coating is introduced in [25, 26], Where it can be beneficial for the detector, filter and sensor of far-infrared range. On the other side, for two related purposes, such as absorber and sensor, a multifunctional nano-imprinted metamaterial surface is synthesized and the metamaterial surface absorption ranges from 100 to 550 nm and provided strong peak absorption [27]. For a complete double band absorber consists of double asymmetric L-shaped graphene resonators, another analysis can be observed. In the mid-infrared field, this form of absorber displayed two and more resonance peaks, where their absorption coefficients are on average greater than 98.77% [28, 29]. An absorptivity rating of almost 100 percent can be achieved with an adjustment spectrum of absorption up to 16 THz as seen in a multi-layered graph structure known as the coherent graphic dependent absorber [7, 30]. In [31], the dialectic surface coats multilayer of graphene to shape the metal resonant multilayer graphene-dielectric-metal flooring system, which essentially shows that the absorbing breadth, as well as the magnitude of the graphene layers, expand dramatically, whereas large graphene layers appear. The absorber architecture as suggested in [33] uses double-layer graph-spectrum, plasmonic field

enhancement and near-field coupling. The new two-layer spatial absorber [34] has been clarified to have maximum absorption and to be calibrated to the infrared spectrum electrically.

Inspired by the properties of the graphene and the metamaterial, we proposed a novel tunable graphene-assisted absorber for the infrared wavelength. The suggested absorber is analyzed for the TE mode of the excitation over a wavelength of 1.5–1.6  $\mu\text{m}$ . The perfect absorption is achieved for multiple short bands. The proposed absorber can be easy to fabricate as it required the fabrication setup for the single-layered graphene silica composition which can be possible with the chemical vapors deposition process.

## 2 Design and modelling

Figure 1 represents a proposed tunable graphene-based absorber structure. Figure 1a shows the three-dimensional outlook of the structure. Figure 1(b) shows the lateral structure view. The proposed structure dimensions are  $L_x = 2\mu\text{m}$ ,  $S_h = 5\mu\text{m}$ ,  $G_x = 1.5\mu\text{m}$ ,  $W = 0.5\mu\text{m}$ ,  $r = 0.1\mu\text{m}$ ,  $W_h = 0.1\mu\text{m}$  and  $S_b = 0.1\mu\text{m}$ . Voltage  $V_g$  regulates the graphene layer. The ground layer and the top of the structure are made of silver (Ag) material. Graphene layers may lead to biomolecular absorption and hence to amplified the local refractive index [32].

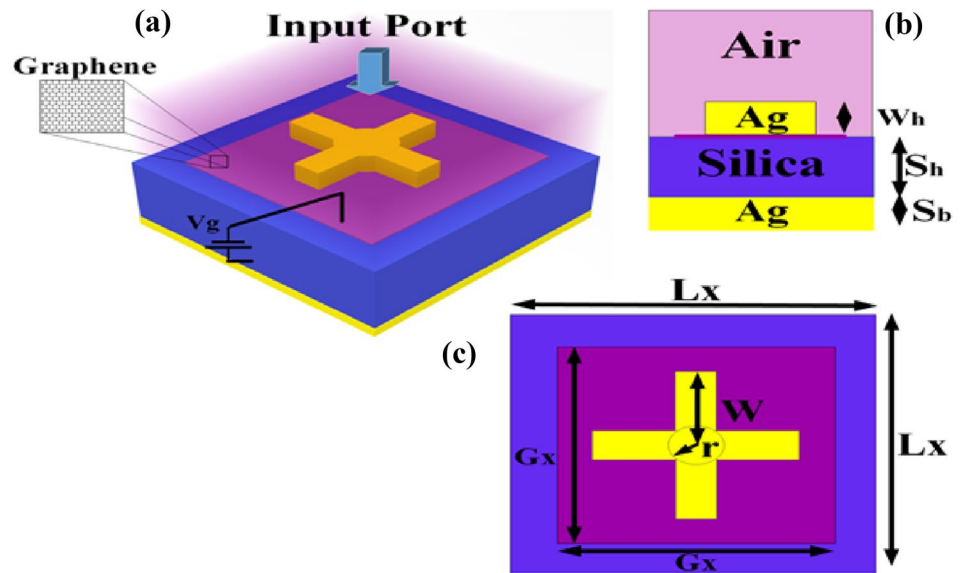
The Kubo formula will express the conductivity values of single-layer graphene [19]. The response of structure also changes by the parameters such as fermi voltage, temperature, frequency, and scattering rate. The permittivity ( $\epsilon(\omega)$ ) of the graphene sheet based on Ref. [33] is shown in Eq. (1). The formula predicting the conductivity of graphene is represented by Eqs. (2 to 4). Graphene was described as a single layer structure in the proposed polarizer structure as a surface conductivity model. The surface current destiny for both of the axis is defined by  $J_x = E_x\sigma_s$  and  $J_y = E_y\sigma_s$ . The structure is investigated for the periodic boundry conditions over X and Y direction. The input wave is incident from the Z direction. The input wave is set on top of the structure from Z direction as illustrated in Fig. 1. The bottom Ag layer is work as mirror for the reflected wave. The material property of the silver is taken form [34]

$$\epsilon(\omega) = 1 + \frac{\sigma_s}{\epsilon_0\omega\Delta} \quad (1)$$

$$\sigma_s = \sigma_{inter} + \sigma_{intra} \quad (2)$$

$$\sigma_{intra} = \frac{-je^2k_B T}{\pi\hbar^2(\omega - j2\Gamma)} \left( \frac{\mu_c}{k_B T} + 2\ln\left(e^{-\frac{\mu_c}{k_B T}} + 1\right) \right) \quad (3)$$

**Fig. 1** Proposed tunable graphene-based absorber structure. **a** Three-dimensional structure view. **b** The structure's side view. **c** Structure top view. The material for the substrate is selected as silica. The top layer of the silica is set as graphene material. The voltage  $V_g$  controls the external voltage of the graphene sheet. The silver (Ag) material forms the ground layer and top resonating structure



$$\sigma_{inter} = \frac{-je^2}{4\pi\hbar} \ln \left( \frac{2|\mu_c| - (\omega - j2\Gamma)\hbar}{2|\mu_c| + (\omega - j2\Gamma)\hbar} \right) \tag{4}$$

$$E_f = \hbar v_F \sqrt{\pi C V_{bg}} \tag{5}$$

$$C = \epsilon_0 \epsilon_d / S_h \tag{6}$$

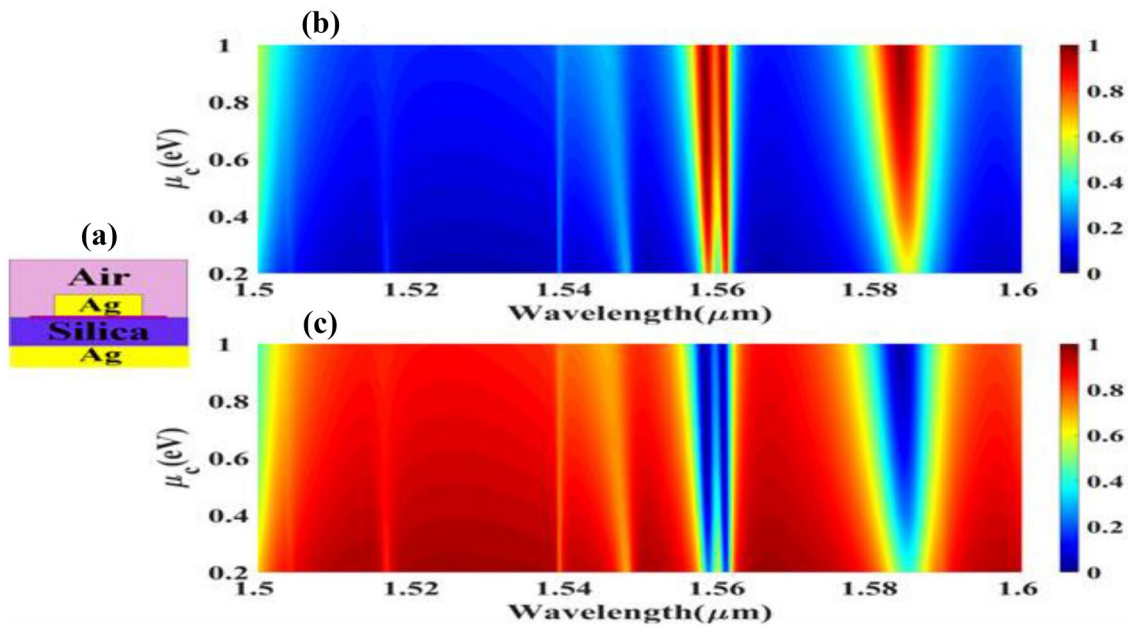
where  $\omega$  is the radian frequency and  $\Gamma$  is the scattering rate. Fermi voltage ( $\mu_c$ ) ranges from 0.2 to 1 eV and it is a bias voltage function of gate terminal is defined by Eq. (5).  $C$  is unit area-wise electrostatic capacitance.  $\epsilon_0$  is the free space permittivity,  $\epsilon_d$  is permittivity (2.25) of the silica material.  $S_h$  is the thickness of the silica layer (5  $\mu\text{m}$ ), Temp. considered is of 300 K, Relaxation time ( $\tau^{-1}$ ) of the electron is  $10^{-13}$  s ( $\tau^{-1} = \Gamma$ ). The basic methods of rendering two-dimensional materials of single-layer graphene substance are Cleavage [35], MBE [36], CVD [37] and techniques. Structure design can be manufactured by a nano-spherical lithograph on the graphene substance top layer [38] and nano-plasmonics lithography [39].

### 3 Results and analysis

The absorption response of the proposed metamaterial-based tunable perfect absorber can be studied into four different stages. We have observed the responses based on a different number of graphene layers, numbers of silicon layers, altering the parameters of the wing structure by concerning the graphene chemical potential variations. Figure 2a represents the absorption for the single-layered graphene silica structure, Figure 2b represents the reflection range of the

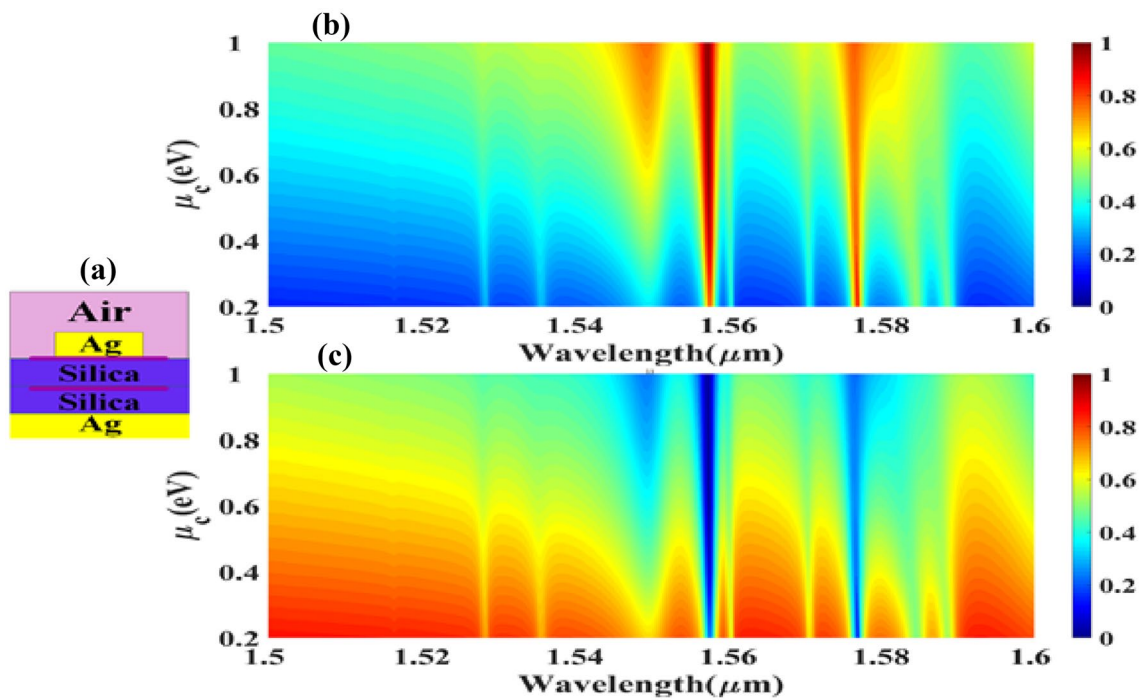
single-layer silica graphene system. The absorption reaction is extracted from the various values of  $\mu_c$ . It is observed that the two narrowband and one wide band of the absorption at 1.56  $\mu\text{m}$  and 1.585  $\mu\text{m}$  wavelength are in a single-layered structure. 99.3% of the highest absorption (HA) for the single-layer structure is observed for  $\mu_c = 0.6$  eV at 1.56  $\mu\text{m}$ . For  $\mu_c = 0.4$  eV, the highest absorption rate is around 94% at 1.56  $\mu\text{m}$ . For  $\mu_c = 0.6$  eV, the highest absorption rate is around 96% at 1.55  $\mu\text{m}$  and 99% at 1.56  $\mu\text{m}$ . For  $\mu_c = 0.8$  eV, the highest absorption rate is around 98% at 1.55  $\mu\text{m}$ , 98% at 1.56  $\mu\text{m}$  and 93% at 1.58  $\mu\text{m}$ . For  $\mu_c = 1$  eV, the highest absorption rate is around 98% at 1.55  $\mu\text{m}$ , 96% at 1.56  $\mu\text{m}$  and 96% at 1.58  $\mu\text{m}$ . The absorption peak is often found to be higher for the upper values of  $\mu_c$ .

Figure 3a, b shows the absorption and reflectance graph for a double layer of graphene. Absorption response is extracted from the various values of  $\mu_c$ . There are two main narrowband responses around wavelength 1.55  $\mu\text{m}$  and 1.57  $\mu\text{m}$ . For  $\mu_c = 0.2$  eV, the highest absorption rate is around 88% at 1.57  $\mu\text{m}$ . For  $\mu_c = 0.4$  eV, the highest absorption rate is around 94% at 1.55  $\mu\text{m}$ . For  $\mu_c = 0.6$  eV, the highest absorption rate is around 99% at 1.55  $\mu\text{m}$ . For  $\mu_c = 0.8$  eV, the HA rate is around 99% at 1.55  $\mu\text{m}$ . For  $\mu_c = 1$  eV, the highest absorption rate is around 98% at 1.55  $\mu\text{m}$ . Figure 4a, b shows the absorption and reflectance graph for a triple layer of graphene for the different values of  $\mu_c$ . The graph indicates three narrowband and a wideband response of the structure. The first narrowband response can be observed at 1.517 and 1.527  $\mu\text{m}$  having 90% absorption for  $\mu_c = 0.2$  eV. The second narrowband response can be observed at 1.516  $\mu\text{m}$  having 96% absorption for  $\mu_c = 0.4$  eV. The third narrowband response can be observed at 1.516  $\mu\text{m}$  having 95% absorption for  $\mu_c = 0.6$  eV. The



**Fig. 2** Absorption and reflection spectra of a single-layered silica graphene design. **a** Side view of a single-layered silica graphene design. **b** Absorption response of proposed design **c** reflectance response for

the proposed design. The perfect absorption was observed at 1.56 and 1.58 μm



**Fig. 3** Absorption and reflection spectra of the two-layer silica graphene design. **a** Side view of the proposed two-layered silica graphene design. **b** Absorption response of proposed design **c** reflectance

response for the proposed design. The perfect absorption is generated near to 1.56 μm and 1.575 μm wavelength. The absorption band is very narrower as compared to the single-layered graphene structure



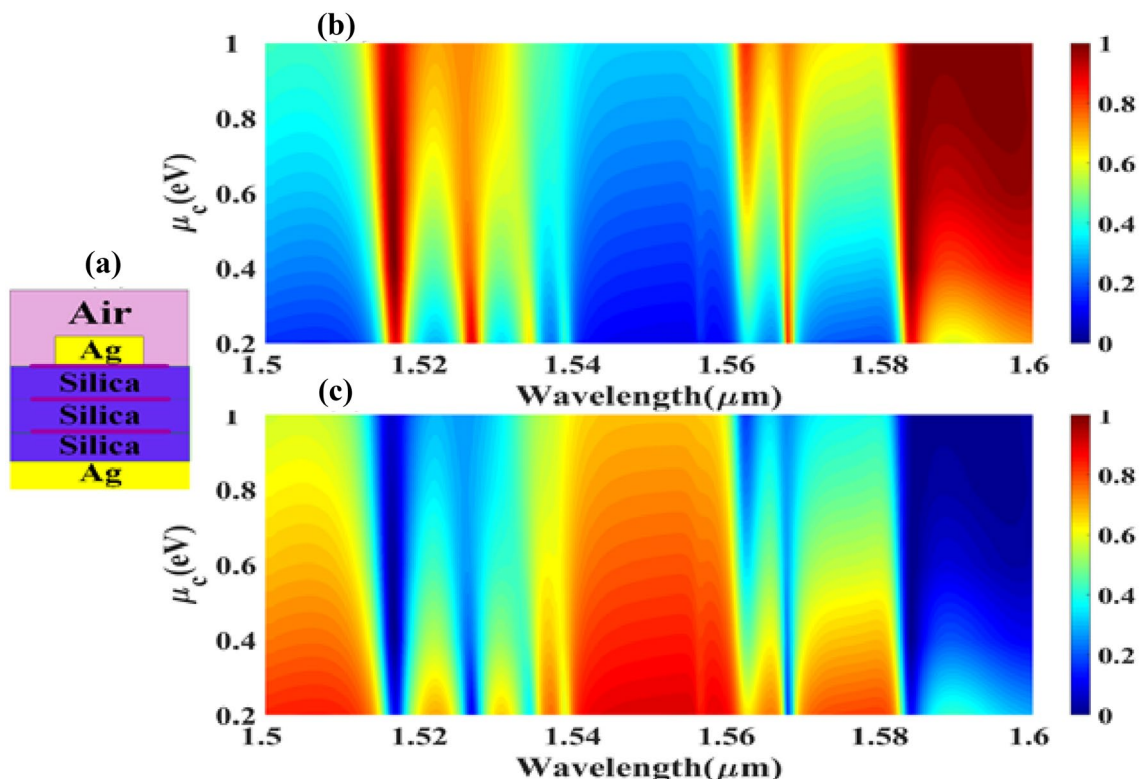


**Fig. 4** Spectra of absorption and reflection of the three-layered design of silica graphene. **a** Side view of the composition of the three-layered silica graphene. **b** Absorption response of proposed design **c** reflectance response for the proposed design. There is a total four

absorption band observed at 1.515 μm, 1.525 μm, 1.565 μm, and 1.58 μm-1.6 μm. The bandwidth of the absorption band is higher for this three-layered structure

third narrowband has an absorption rate lower than the other two bands. The wideband response for the triple-layer can be observed from the range of 1.58 to 1.6 μm. The highest average absorption rate for the different chemical potential ( $\mu_c$  0.6, 0.8 and 1 are respectively 99.71%, 99.71% and 99.92%.

Figure 5 represents the behavior of absorption and reflection property of four-layered silicon graphene design. Four narrow bands are observed. The highest absorption is about 90% at 1.56 μm, 92% at 1.539 μm, 91% at 1.58 μm for  $\mu_c=0.2$  eV. The highest absorption is about 93.5% at 1.539 μm, 91.7% at 1.564 μm, 90% at 1.581 μm for the  $\mu_c=0.4$  eV. The highest absorption is about 94% at 1.56 μm, 87% at 1.582 μm for  $\mu_c=0.6$  eV. The highest absorption is about 93% at 1.563 μm, 93.5% at 1.563 μm for the  $\mu_c=1$  eV. It is clarified that an increase number of silicon graphene layers will increase the number of narrow bands. Figure 6 represents the absorption of the proposed design by the variations of the radius of structure for the range 200 nm to 500 nm. The highest absorption is about 94% at 1.55 μm, 92% at 1.56 μm, 91.5% at 1.56 μm, 91.2% at 1.58 μm for  $r=200$  nm. The highest absorption is about 95% at 1.54 μm, 92% at 1.56 μm,

91% at 1.55 μm for  $r=300$  nm. The highest absorption is about 85% at 1.50 μm, 95% at 1.53 μm, 97% at 1.55 μm and 90% at 1.59 μm for  $r=400$  nm. The highest absorption is about 94% at 1.527 μm for  $r=500$  nm.

The perfect absorption in the proposed structure is generated because the resonance and electric field concentration increase at a specific wavelength. The rise in the electric field concentration because of the impedance matching between two materials results in the strong dipole moment generation [40]. The impedance matching condition generates the variation in the refractive index. The real and imaginary parts of the refractive index variation will ultimately result in high absorption or reflectance amplitude generation. Narrowband and wideband of the absorption spectrum are generated because of the variation in chemical potential and the constructive/destructive field concentration at the graphene patch sheet. The comparative analysis of all types of graphene silica layered structure is presented in Table 1. The comparative Table is clarifies the variation in terms of the number of bands, graphene chemical potential, and absorption band range.

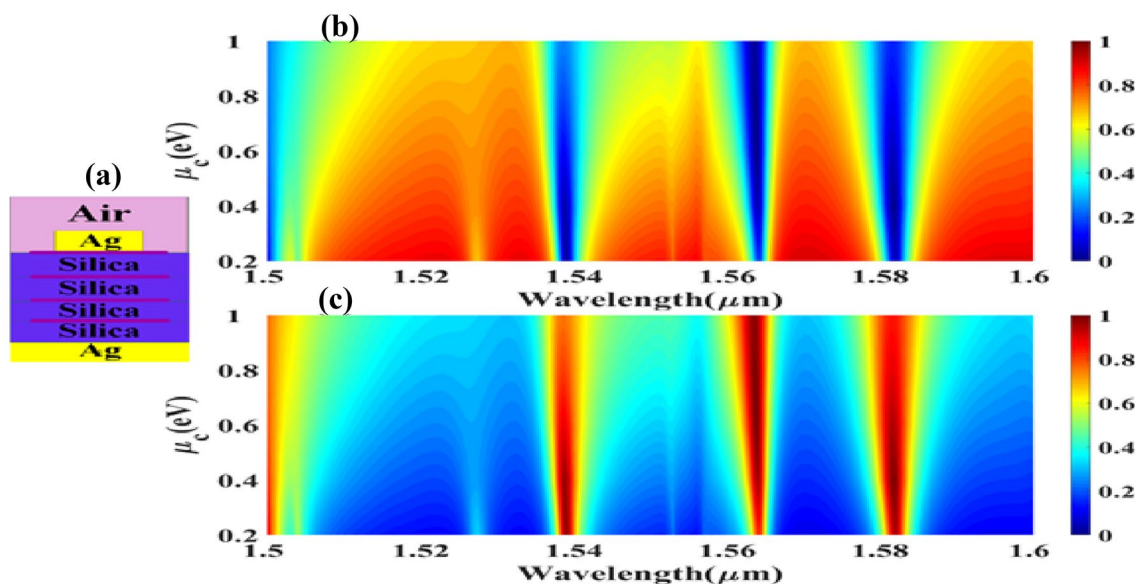
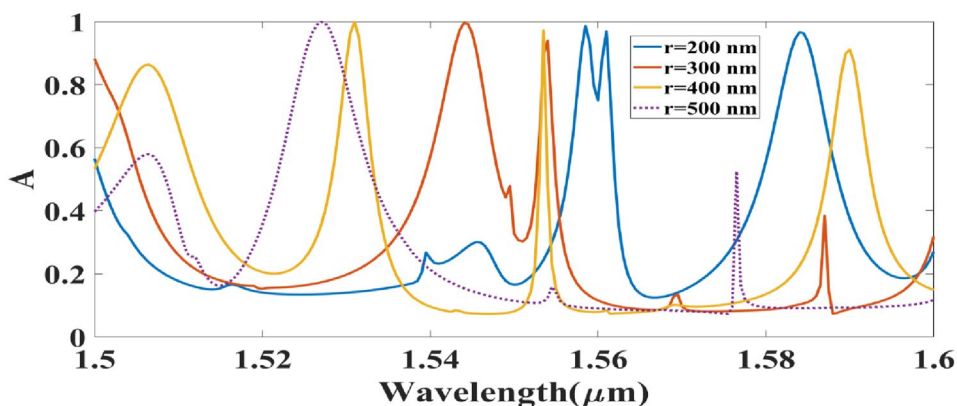


**Fig. 5** Spectra of absorption and reflection of the four-layered design of silica graphene. **a** Side view of the composition of the four-layered silica graphene. **b** Absorption response of proposed design **c** reflectance response for the proposed design. There is three absorption

band observed in the four-layered structure at 1.54  $\mu\text{m}$ , 1.565  $\mu\text{m}$ , and 1.58  $\mu\text{m}$ . The graphene chemical potential of the graphene sheet is a tunable parameter for controlling the absorption peaks

**Fig. 6** Absorption for various resonator radius values is mentioned as  $r$  in Fig. 1c. The circle radius varies between 200 to 500 nm



The range of the absorption in this Table is considered for >85% of amplitude. It is clarified that for the different chemical potential values the absorption wavelength range is different.

Figure 7 represents the absorption of the proposed structure is also analyzed by the variations of width ( $w$ ) of structure for the range 200 nm to 400 nm. The highest absorption is about 92% at 1.54  $\mu\text{m}$  for  $W = 200$  nm. The highest absorption is about to 86% at 1.50  $\mu\text{m}$ , 94% at 1.543  $\mu\text{m}$ , 91% at 1.55  $\mu\text{m}$ , for  $W = 300$  nm. The highest absorption is about 89% at 1.50  $\mu\text{m}$ , 94% at 1.54  $\mu\text{m}$  for  $W = 400$  nm. Figure 8 represents the absorption of suggested structure is also investigated by the height of silver ( $W_h$ ) resonator for the range 100 nm to 600 nm. The respective highest absorption

is 99.8% at 1.544  $\mu\text{m}$  for  $w_h = 100$  nm, 99.8% at 1.55  $\mu\text{m}$  for  $w_h = 200$  nm, 85% at 1.578  $\mu\text{m}$  and 90% at 1.598  $\mu\text{m}$  for  $w_h = 200$  nm, 99% at 1.6  $\mu\text{m}$  for  $w_h = 400$  nm.

Figure 9 represents the height of silica substrate ( $S_h$ ) ranges from 200 to 1200 nm for the rate of absorption analysis. The highest absorption are 92% at 1.55  $\mu\text{m}$  and 99% at 1.568  $\mu\text{m}$  for  $S_h = 200$  nm, 97% at 1.571  $\mu\text{m}$  for  $S_h = 400$  nm, 84% at 1.517  $\mu\text{m}$  and 97% at 1.564  $\mu\text{m}$  for  $S_h = 600$  nm, 90% at 1.564  $\mu\text{m}$  for  $S_h = 800$  nm, 92% at 1.554  $\mu\text{m}$  for  $S_h = 1000$  nm, 83% at 1.55  $\mu\text{m}$ , 97% at 1.554  $\mu\text{m}$  and 99.9 at 1.565  $\mu\text{m}$  for  $S_h = 1200$  nm. Figure 10 represents the absorption observed for the  $2 \times 2$  array structure for the variations of the chemical potential in the range of 0.2 to 1. The maximum absorption of 93% at 1.505  $\mu\text{m}$  and 99.8% at

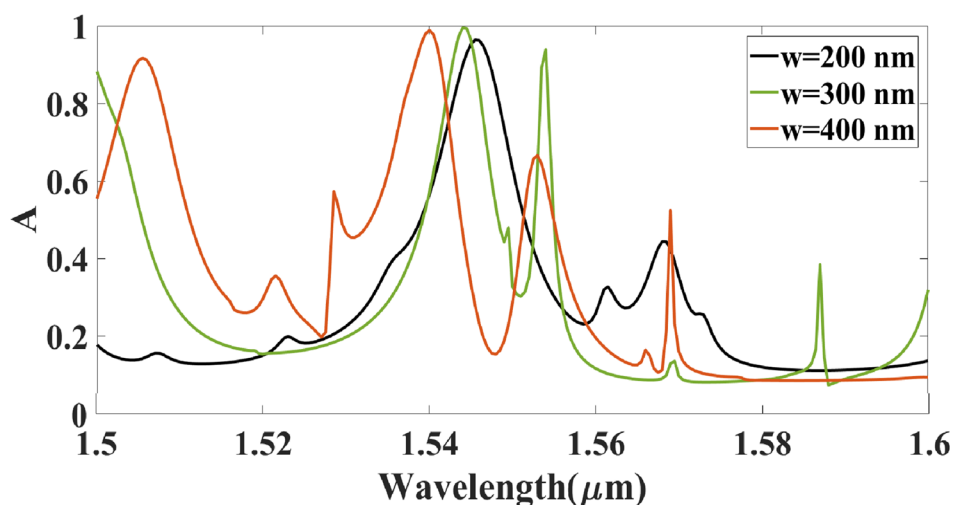
**Table 1** Comparative table of all structures with number of absorption bands, chemical potential, and absorption range (> 85%)

Number of Graphene layered structure	Number of Bands	Chemical Potential (eV)	Wavelength Range (μm)
1	3	1	1.558–1.559
		1	1.560–1.561
		1	1.582–1.585
2	2	0.2	1.576–1.577
		1	1.556–1.558
3	3	1	1.515–1.518
		0.2	1.526–1.527
		1	1.583–1.6
4	4	0.2	1.5–1.501
		0.4	1.538–1.540
		1	1.562–1.564
		0.8	1.581–1.583

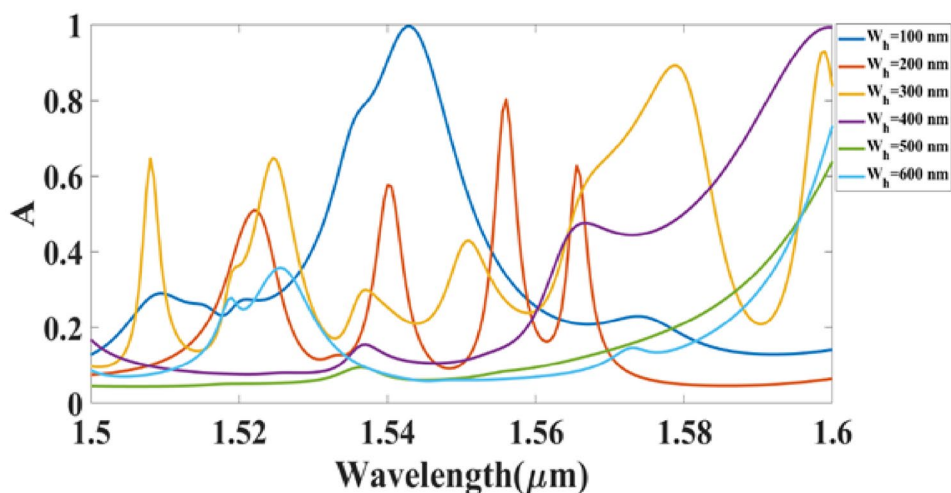
1.522 μm for  $\mu_c = 0.2\text{eV}$ . The maximum absorption of 89% at 1.504 μm and 91% at 1.522 μm for  $\mu_c = 0.4\text{eV}$ . The maximum absorption of 80% at 1.5 μm for  $\mu_c = 0.6\text{eV}$ . The maximum absorption (MA) of 84% at 1.5 μm for  $\mu_c = 0.8\text{eV}$ . The MA of 85% at 1.5 μm for  $\mu_c = 1\text{eV}$ .

Figure 11 represents absorption for the 3 × 3 array structure for the variations of chemical potential in the range of 0.2 to 1. Array structure of 3 × 3 provides a wide band spectrum for the chemical potential ( $\mu$  0.6 to 1. More than 80% absorption observed for the range 1.5150 μm to 1.5190 μm for the  $\mu_c = 0.6\text{eV}$ , 1.5135 μm to 1.5200 μm for the  $\mu_c = 0.8\text{eV}$  and 1.5125 μm to 1.5205 μm for the  $\mu_c = 1\text{eV}$ . Transmission and reflection values use for the refractive index calculation of the proposed absorption structure expression suggested in [41]. Figure 12 shows the calculated refractive indices for the proposed designs of the absorber structure. It is detected that the effective refractive index values at different resonance peaks become negative. This effect proves the behavior of the different designs of the proposed absorber stature as a metamaterial. In general, the refractive index

**Fig. 7** Absorption for various resonator width values is mentioned as w in Fig. 1c. The width of the resonating wing varies between 200 to 400 nm



**Fig. 8** Absorption for various height of silica resonator values is mentioned as Wh in Fig. 1c. The silica substrate height changes between 100 to 600 nm



**Fig. 9** Absorption for the various silica layer height values is mentioned as  $S_h$  in Fig. 1c. The silica substrate height changes from 200 to 1200 nm

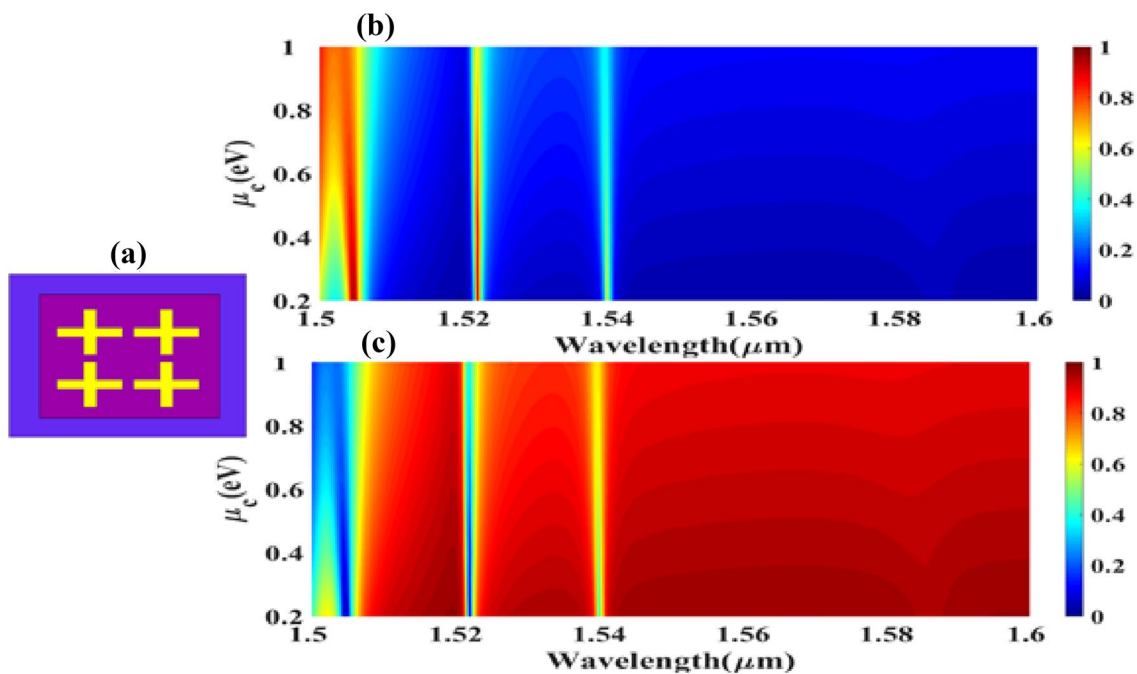
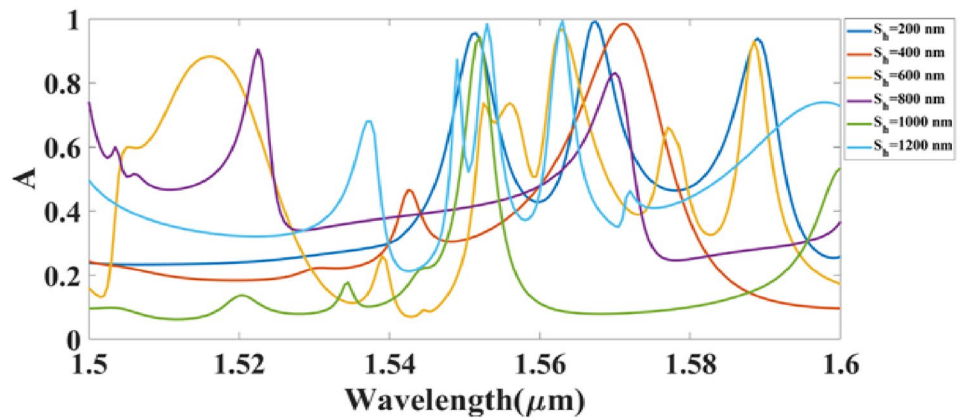


**Fig. 10** Absorption and reflection spectra of  $2 \times 2$  array structure of the top resonator. **a** Top view of the proposed  $2 \times 2$  array structure. **b** Absorption and **c** reflectance response for the proposed design. The

other proportions of the entire design are kept the same as defined in Fig. 1. The dimension of the resonator was reduced by a scaling factor of 2 for  $2 \times 2$  geometry

values of the entire structure affect absorption and reflectance. The refractive index imaginary part contributes to absorption while the real part contributes to reflectance. As presented in Fig. 12, all the absorption peak is generated at the places where the refractive indices real part reduces and refractive indices imaginary part increases. This effect is observed in all the structures. These effects are generated because of the light interaction between two mediums from Air-Ag and Air-Ag-Graphene.

The metamaterial effect of the proposed structure is generated due to the dipole moment generated at various

resonating points as illustrated in Fig. 13. The propagation properties of electromagnetic fields suggest magnetic dipoles can be caused to release radiation [42]. Figure 13 represents normalized electric field intensity with surface current distribution on the cut plane of XY direction for the single-layer graphene structure. Every resonance point-wise dipole moment is observed on the graphene surface. Resonance points of electric field intensity are located on  $1.447 \mu\text{m}$ ,  $1.559 \mu\text{m}$ ,  $1.561 \mu\text{m}$  and  $1.585 \mu\text{m}$ . Figure 14 shows the absorption and reflectance amplitude of the different array structure that is placed on the upper side of



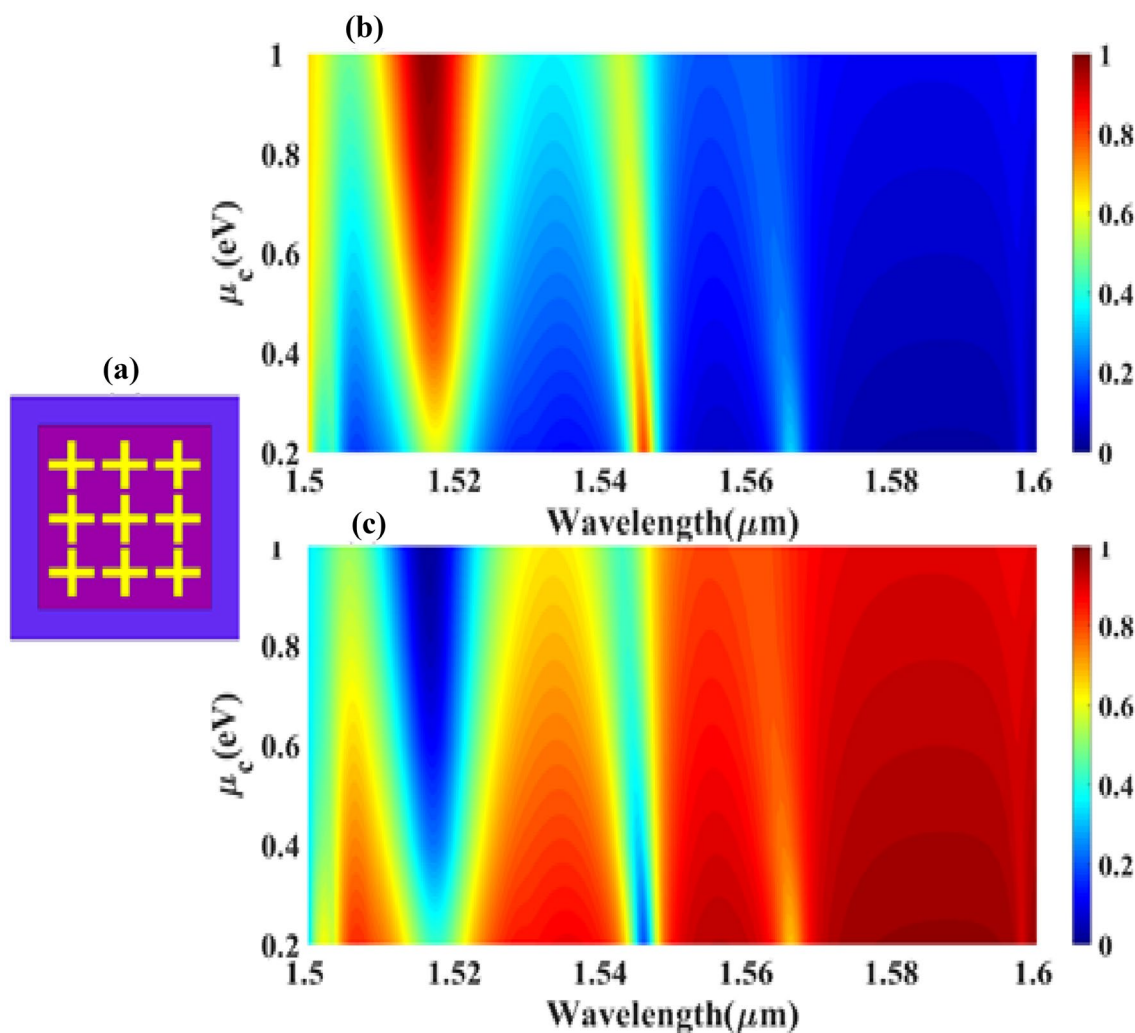


**Fig. 11** Absorption and reflection spectra of  $3 \times 3$  array structure of the top resonator. **a** Top view of the proposed  $3 \times 3$  array structure. **b** Absorption response **c** reflectance response for the proposed design.

The other dimensions of the entire structure are kept the same as defined in Fig. 1. The dimension of the resonator is reduced by a scaling factor of 3 for  $3 \times 3$  geometry

the graphene sheet. Figure 14 is derived for the single-layered graphene silica-based structure. It is visualized that the absorption peaks are varied for all the resonating arrays. The higher array of the same size results in the multiple absorption peaks due to the multiple dipole moment generations.

Figure 15 clarifies the absorption peak variation for the different material conditions. The absorption spectrum is investigated for the three conditions, (i) single-layer graphene structure as illustrated in Fig. 2, (ii) Without graphene structure, (iii) Without graphene structure with gold (Au) as resonator structure. It is clarified that the resonance peaks are different for every material condition. It is also clarified that the resonance conditions with graphene structure are

also different as compared to the without graphene structure. The graphene-based structure provided the flexibility to tune the resonating band in terms of absorption amplitude which was not directly possible with other materials. Ag and graphene patch both generates the dipole moments as shown in Fig. 13 which is the main reason to generate the high concentrated field at a specific wavelength point. Hence the graphene and resonating Ag offer the constructive resonating condition over  $1.5\text{--}1.6\ \mu\text{m}$  range of the wavelength. Figure 16 shows the variation in the absorption for various sizes of the graphene patch. It is clarified that the variation in the absorption is large for various sizes of the graphene patch. The reason for the large variation is because of the impedance matching values and dipole

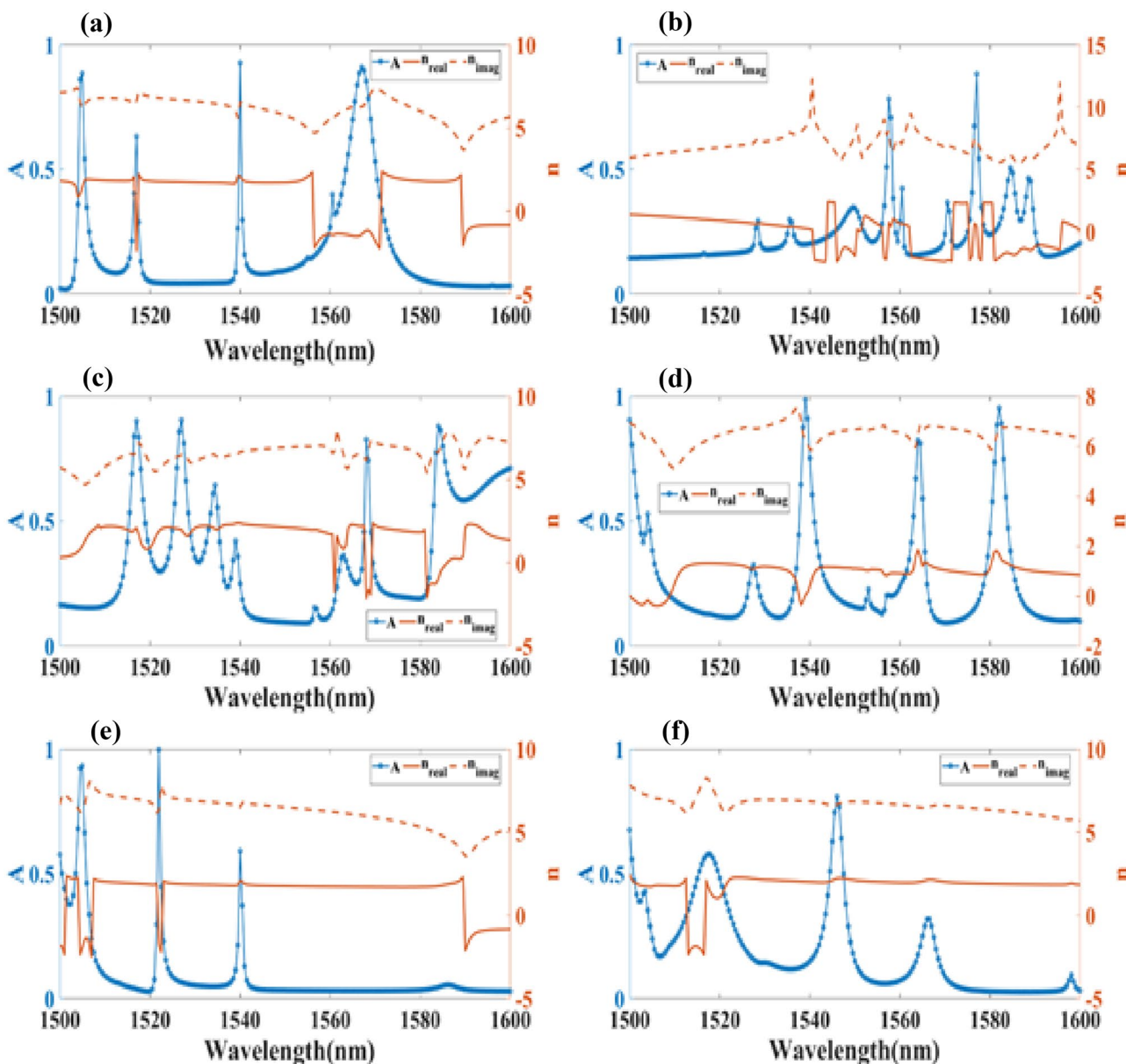


**Fig. 12** Absorption, real refractive index and imaginary refractive index values for the different proposed structures. Refractive index and variation in the absorption for **a** one layered graphene, **b** two-layered

graphene, **c** three-layered graphene, **d** four-layered graphene, **e**  $2 \times 2$  array structure **f**  $3 \times 3$  array structures

moment response is different for the different size of the graphene patch. The fabricated response is going to differ if the variation in graphene size. In terms of fabrication tolerance, the shape of the graphene is a major factor to identify the resonance bandwidth. Other parameters such as resonator shape, substrate high are also affecting resonance conditions. To achieve the perfect absorption and at a specific wavelength, we can choose the suitable parameters presented in the manuscript.

Comparative research with previously published work of the proposed framework is represented in Table 2. Comparative research of various layered structures is conducted based on structure dimensions, operational wavelength, total absorption value, and material.

Sila (single layer), Mula (multi-layer), Ag (silver), Si (silica), Gr (graphene), M (metal), D (dielectric), Au (gold), Al (aluminum).

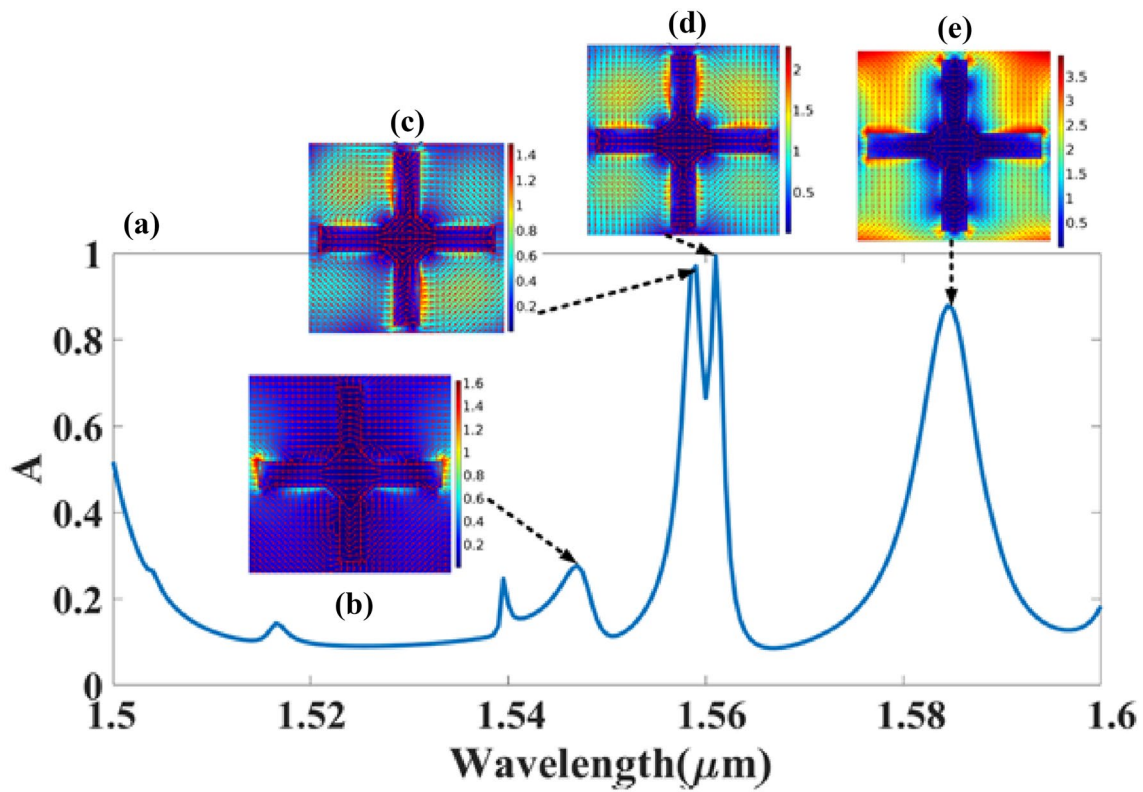


Fig. 13 Normalized electric field intensity with surface current distribution on the cut plane of XY direction. **a** Absorption for the one-layer absorber structure. Electric field intensity at **a** 1.447  $\mu\text{m}$ . **b** 1.559  $\mu\text{m}$ , **c** 1.561  $\mu\text{m}$ , **d** 1.585  $\mu\text{m}$  resonating peaks

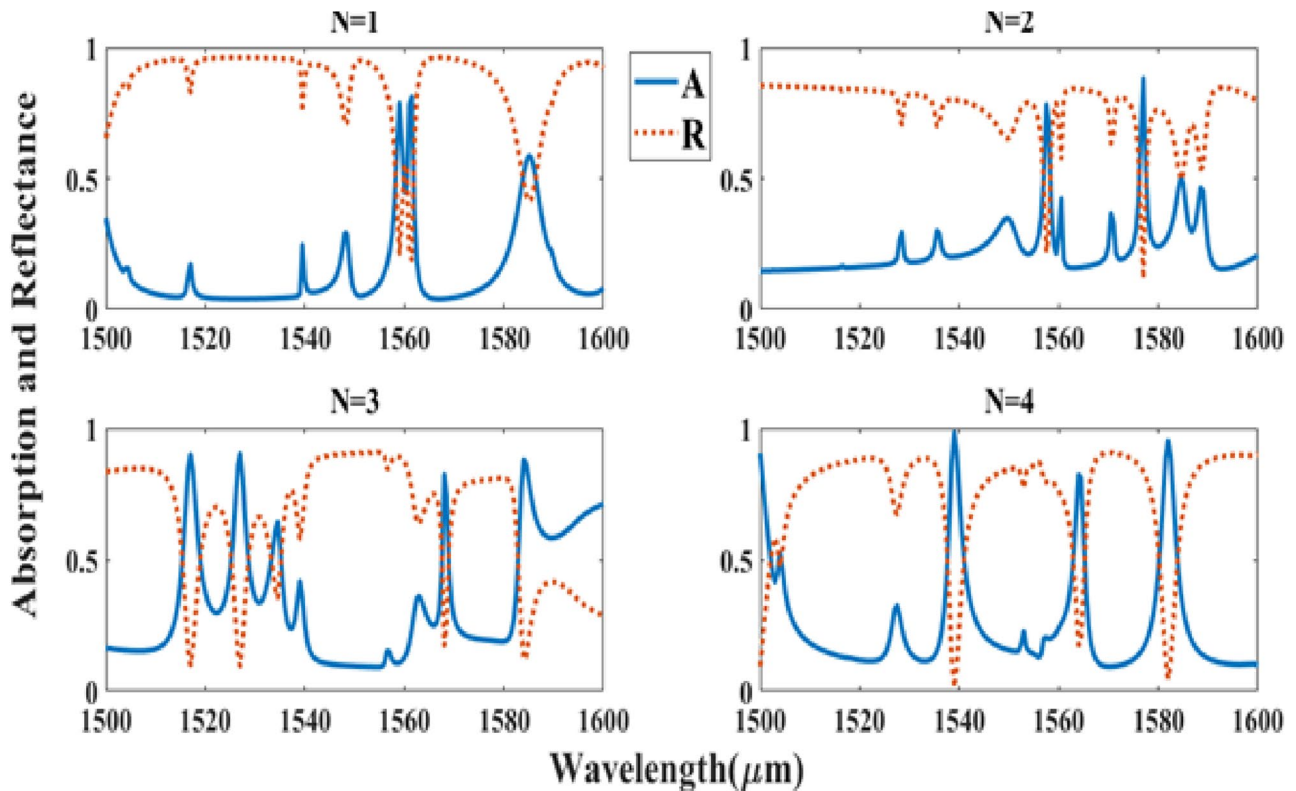
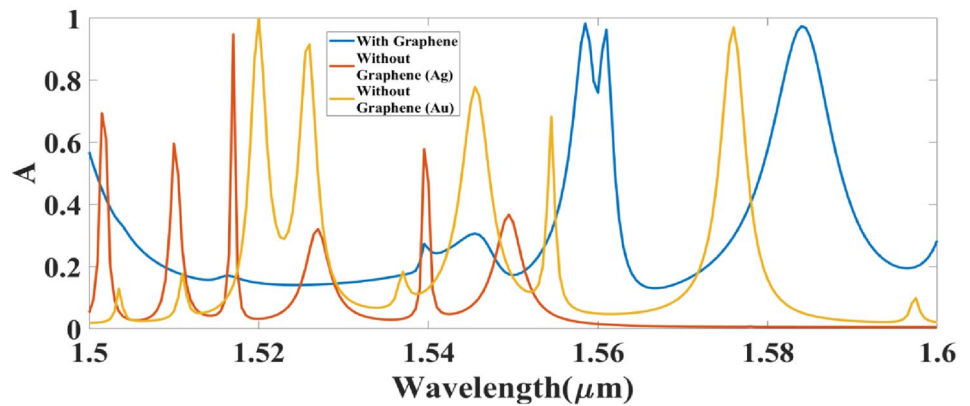
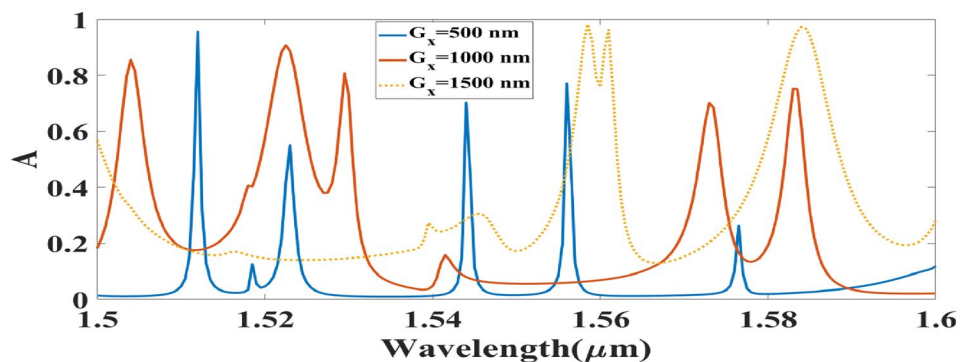


Fig. 14 Comparative analysis of absorption and reflectance for the different layered graphene silica designs. N defined the number of the graphene silica layer

**Fig. 15** Comparative absorption spectrum for the various conditions of the materials



**Fig. 16** Absorption for various shapes of the graphene patch for identifying the tolerance and dependency on graphene shape



**Table 2** Comparative research with other recently published studies

References	Number of layers	Materials	Dimensions of structure	Operating band ( $\mu\text{m}$ )	Peak absorption
Proposed work	SiLa and MuLa	Ag-Gr-Si-Ag	$2 \times 2 \times 0.5 \mu\text{m}^3$	1.5 to 1.6	~99%
[43]	Sila	Gr-Si-D	$2.5 \times 2.5 \times 0.3 \mu\text{m}^3$	20 to 40	~20%
[44]	MuLa	D-M	$0.32 \times 0.9 \times 0.8 \mu\text{m}^3$	1.4 to 1.7	~90%
[45]	MuLa	M	$0.104 \times 0.052 \times 0.16 \mu\text{m}^3$	0.4 to 0.6	~97%
[46]	SiLa	Au	$0.3 \times 0.5 \mu\text{m}^2$	1.8 to 2.4	~95%
[27]	Mula	D-M-Au	$0.3 \times 0.3 \times 0.74 \mu\text{m}^3$	9 to 14.0	~99%
[47]	Sila	M-T-Si-Ag	$0.48 \times 0.48 \times 0.3 \mu\text{m}^3$	0.7 to 1	~95%
[48]	Mula	Al-D	$70 \times 70 \times 72 \mu\text{m}^3$	150 to 200	~98%
[49]	Sila	Al-D-Au	–	1.6 to 3	~99%
[50]	Mula	D-Au-MgF <sub>2</sub>	$0.6 \times 0.6 \times 0.6 \mu\text{m}^3$	1.36 to 2.14	~99%
[51]	Sila	M-D-Ag	$0.09 \times 0.05 \times 0.09 \mu\text{m}^3$	2.4 to 3.2	~98%

## 4 Conclusion

In conclusion, graphene-based tunable short-band absorbers have been numerically examined for the infrared wavelength changes from 1.5 to 1.6  $\mu\text{m}$ . The absorption behaviour of one layer, dual-layer, three-layer, as well four-layer graphene-based structures has been analyzed. The tunability of the proposed absorber has been controlled by the graphene Fermi/chemical potential that can further

be adjusted by an external power supply. It is clarified that more silicon graphene layers will increase the narrow bands. All proposed structures provide metamaterial behavior. It is clarified that 99% of the absorption amplitude in single, double, and triple-layer structures can be happened. The structure is also compared with the structure where the graphene is absent to identify the change in the absorption. It is identified that the graphene-based absorption structure will give the constructive resonating



effect with a tunable resonating band facility. The proposed absorber structure is compact and easy for experimental studies because of the simple layered architecture. This structure can become part of the large THz photonics system that works in the infrared domain.

**Acknowledgements** The authors would like to acknowledge the support received from Taif University Researchers Supporting Project Number (TURSP-2020/147), Taif university, Taif, Saudi Arabia.

## Declarations

**Conflict of interest** All the authors approved this submission and have no competing interests.

## References

- J.C. Bose, On the rotation of plane of polarisation of electric wave by a twisted structure. *Proc. R. Soc. Lond.* **63**, 146–152 (1898). <https://doi.org/10.1098/rspl.1898.0019>
- I. V. Lindell, A.H. Sihvola, J. Kurkijärvi, K.F. Lindman, The last Hertzian, and a Harbinger of electromagnetic chirality. *IEEE Antennas Propag. Magn.* **34**, 24–30 (1992). <https://doi.org/10.1109/74.153530>
- W.E. Kock, Metallic delay lenses. *Bell Syst. Tech. J.* **27**, 58–82 (1948). <https://doi.org/10.1002/j.1538-7305.1948.tb01331.x>
- D.R. Smith, S. Schultz, P. Markoš, C.M. Soukoulis, Determination of effective permittivity and permeability of metamaterials from reflection and transmission coefficients. *Phys. Rev. B Condens. Matter Mater. Phys.* **65**, 1–5 (2002). <https://doi.org/10.1103/PhysRevB.65.195104>
- T.J. Cui, R. Liu, D.R. Smith, Introduction to metamaterials, in: *Metamaterials Theory, Des. Appl.*, Springer US, 2010: pp. 1–19. doi:[https://doi.org/10.1007/978-1-4419-0573-4\\_1](https://doi.org/10.1007/978-1-4419-0573-4_1)
- V.G. Veselago, The electrodynamics of substances with simultaneously negative values of  $\epsilon$  and  $\mu$ . *Sov. Phys. Uspekhi.* **10**, 509–514 (1968). <https://doi.org/10.1070/PU1968v010n04ABEH003699>
- V. Sorathiya, V. Dave, Numerical study of a high negative refractive index based tunable metamaterial structure by graphene split ring resonator for far infrared frequency. *Opt. Commun.* **456**, 124581 (2020). <https://doi.org/10.1016/j.optcom.2019.124581>
- R. Singh, E. Plum, W. Zhang, N.I. Zheludev, Highly tunable optical activity in planar achiral terahertz metamaterials. *Opt. Express.* **18**, 13425 (2010). <https://doi.org/10.1364/oe.18.013425>
- J.B. Pendry, Negative refraction makes a perfect lens. *Phys. Rev. Lett.* **85**, 3966–3969 (2000). <https://doi.org/10.1103/PhysRevLett.85.3966>
- D. Schurig, J.J. Mock, B.J. Justice, S.A. Cummer, J.B. Pendry, A.F. Starr, D.R. Smith, Metamaterial electromagnetic cloak at microwave frequencies. *Science* (80). **314**, 977–980 (2006). doi:<https://doi.org/10.1126/science.1133628>
- H.F. Ma, T.J. Cui, Three-dimensional broadband ground-plane cloak made of metamaterials. *Nat. Commun.* **1**, 1–6 (2010). <https://doi.org/10.1038/ncomms1023>
- T. Ergin, N. Stenger, P. Brenner, J.B. Pendry, M. Wegener, Three-dimensional invisibility cloak at optical wavelengths. *Science* (80). **328**, 337–339 (2010). <https://doi.org/10.1126/science.1186351>
- A.K. Geim, K.S. Novoselov, The rise of graphene. *Nat. Mater.* **6**, 183–191 (2007). <https://doi.org/10.1038/nmat1849>
- L.A. Falkovsky, Optical properties of grapheme. *J. Phys. Conf. Ser.* **129** (2008). doi:<https://doi.org/10.1088/1742-6596/129/1/012004>.
- E. Pop, V. Varshney, A.K. Roy, Thermal properties of graphene: fundamentals and applications. *MRS Bull.* **37**, 1273–1281 (2012). <https://doi.org/10.1557/mrs.2012.203>
- K.I. Bolotin, K.J. Sikes, Z. Jiang, M. Klima, G. Fudenberg, J. Hone, P. Kim, H.L. Stormer, Ultrahigh electron mobility in suspended graphene. *Solid State Commun.* **146**, 351–355 (2008). <https://doi.org/10.1016/j.ssc.2008.02.024>
- L. Ju, B. Geng, J. Horng, C. Girit, M. Martin, Z. Hao, H.A. Bechtel, X. Liang, A. Zettl, Y.R. Shen, F. Wang, Graphene plasmonics for tunable terahertz metamaterials. *Nat. Nanotechnol.* **6**, 630–634 (2011). <https://doi.org/10.1038/nnano.2011.146>
- X. He, S. Kim, Graphene-supported tunable waveguide structure in the terahertz regime. *J. Opt. Soc. Am. B.* **30**, 2461 (2013). <https://doi.org/10.1364/josab.30.002461>
- G.W. Hanson, Dyadic Green's functions and guided surface waves for a surface conductivity model of graphene. *J. Appl. Phys.* **103** (2008). doi:<https://doi.org/10.1063/1.2891452>
- L. Hu, H. Dai, F. Xi, Y. Tang, F. Cheng, Enhanced circular dichroism in hybrid graphene–metal metamaterials at the near-infrared region. *Opt. Commun.* **473**, 125947 (2020). <https://doi.org/10.1016/j.optcom.2020.125947>
- M.S. Islam, J. Sultana, M. Biabanifard, Z. Vafapour, M.J. Nine, A. Dinovitser, C.M.B. Cordeiro, B.W.H. Ng, D. Abbott, Tunable localized surface plasmon graphene metasurface for multiband superabsorption and terahertz sensing. *Carbon N. Y.* **158**, 559–567 (2020). <https://doi.org/10.1016/j.carbon.2019.11.026>
- A. Alipour, A. Mir, A. Farmani, Ultra high-sensitivity and tunable dual-band perfect absorber as a plasmonic sensor. *Opt. Laser Technol.* **127**, 106201 (2020). <https://doi.org/10.1016/j.optlastec.2020.106201>
- X. Jiang, Z. Zhang, K. Wen, G. Li, J. He, J. Yang, A triple-band hybridization coherent perfect absorber based on graphene metamaterial. *Appl. Sci.* **10**, 1750 (2020). <https://doi.org/10.3390/app10051750>
- J. Zhang, Q. Hong, J. Zou, Y. He, X. Yuan, Z. Zhu, S. Qin, Fano-resonance in hybrid metal-graphene metamaterial and its application as mid-infrared plasmonic sensor. *Micromachines.* **11**, 268 (2020). <https://doi.org/10.3390/mi11030268>
- H. Lin, X. Ye, X. Chen, Z. Zhou, Z. Yi, G. Niu, Y. Yi, Y. Hua, J. Hua, S. Xiao, Plasmonic absorption enhancement in graphene circular and elliptical disk arrays. *Mater. Res. Express.* **6**, 045807 (2019). <https://doi.org/10.1088/2053-1591/aafc3e>
- L. Thomas, V. Sorathiya, S.K. Patel, T. Guo, Graphene-based tunable near-infrared absorber. *Microw. Opt. Technol. Lett.* **61**, 1161–1165 (2019). <https://doi.org/10.1002/mop.31712>
- M. Freitag, W. Zhu, P. Avouris, F. Xia, H. Yan, X. Li, B. Chandra, G. Tulevski, Y. Wu, Tunable infrared plasmonic devices using graphene/insulator stacks. *Nat. Nanotechnol.* **7**, 330–334 (2012). <https://doi.org/10.1038/nnano.2012.59>
- S. Xia, M. Qin, X. Zhai, Y. Xiang, L. Wang, Q. Lin, Tunable dual-band perfect absorber based on L-shaped graphene resonator. *IEEE Photon. Technol. Lett.* **31**, 483–486 (2019). <https://doi.org/10.1109/LPT.2019.2900269>
- V. Sorathiya, S.K. Patel, D. Katrodiya, C. Jani, Metasurface based broadband solar absorber. *Opt. Mater. (Amst)* **89**, 34–41 (2019). <https://doi.org/10.1016/j.optmat.2018.12.057>
- X. Han, H. Chen, H. Zhou, X. Jin, F. Wang, S. Huang, Z. Xie, L. Li, Coherent perfect absorber with independently tunable frequency based on multilayer graphene. *Opt. Commun.* **446**, 44–50 (2019). <https://doi.org/10.1016/j.optcom.2019.04.043>

31. L. Qi, C. Liu, Broadband multilayer graphene metamaterial absorbers. *Opt. Mater. Express.* **9**, 1298 (2019). <https://doi.org/10.1364/ome.9.001298>
32. I. Pockrand, Surface plasma oscillations at silver surfaces with thin transparent and absorbing coatings. *Surf. Sci.* **72**, 577–588 (1978). [https://doi.org/10.1016/0039-6028\(78\)90371-0](https://doi.org/10.1016/0039-6028(78)90371-0)
33. J. Jiang, Q. Zhang, Q. Ma, S. Yan, F. Wu, X. He, Dynamically tunable electromagnetically induced reflection in terahertz complementary graphene metamaterials. *Opt. Mater. Express.* **5**, 1962 (2015). <https://doi.org/10.1364/ome.5.001962>
34. R.W. Christy, P.B. Johnson, Optical constants of the noble metals. *Phys. Rev. B.* **6**, 4370–4379 (1972). <https://doi.org/10.1016/j.susc.2018.02.016>
35. V.V. Khotkevich, S.V. Morozov, A.K. Geim, K.S. Novoselov, D. Jiang, F. Schedin, T.J. Booth, Two-dimensional atomic crystals. *Proc. Natl. Acad. Sci.* **102**, 10451–10453 (2005). <https://doi.org/10.1073/pnas.0502848102>
36. J. Avila, M.C. Asensio, F. Bournel, J.-J. Gallet, E. Moreau, S. Godey, F.J. Ferrer, D. Vignaud, X. Wallart, Graphene growth by molecular beam epitaxy on the carbon-face of SiC. *Appl. Phys. Lett.* **97**, 241907 (2010). <https://doi.org/10.1063/1.3526720>
37. N. Petrone, C.R. Dean, I. Meric, A.M. van der Zande, P.Y. Huang, L. Wang, D. Muller, K.L. Shepard, J. Hone, Chemical vapor deposition-derived graphene with electrical performance of exfoliated graphene. *Nano Lett.* **12**, 2751–2756 (2012). <https://doi.org/10.1021/nl204481s>
38. M.C. Sherrott, P.W.C. Hon, K.T. Fountaine, J.C. Garcia, S.M. Ponti, V.W. Brar, L.A. Sweatlock, H.A. Atwater, Experimental demonstration of >230° phase modulation in gate-tunable graphene-gold reconfigurable mid-infrared metasurfaces. *Nano Lett.* **17**, 3027–3034 (2017). <https://doi.org/10.1021/acs.nanolett.7b00359>
39. T. Zou, B. Zhao, W. Xin, Y. Wang, B. Wang, X. Zheng, H. Xie, Z. Zhang, J. Yang, C.L. Guo, High-speed femtosecond laser plasmonic lithography and reduction of graphene oxide for anisotropic photoresponse. *Light Sci. Appl.* **9** (2020). doi:<https://doi.org/10.1038/s41377-020-0311-2>.
40. H. Huang, H. Xia, Z. Guo, D. Xie, H. Li, Dynamically tunable dendritic graphene-based absorber with thermal stability at infrared regions. *Appl. Phys. A Mater. Sci. Process.* **124**, 429 (2018). <https://doi.org/10.1007/s00339-018-1844-6>
41. D.R. Smith, W.J. Padilla, D.C. Vier, S.C. Nemat-Nasser, S. Schultz, Composite medium with simultaneously negative permeability and permittivity. *Phys. Rev. Lett.* **84**, 4184–4187 (2000). <https://doi.org/10.1103/PhysRevLett.84.4184>
42. J. Chen, S. Chen, P. Gu, Z. Yan, C. Tang, Z. Xu, B. Liu, Z. Liu, Electrically modulating and switching infrared absorption of monolayer graphene in metamaterials. *Carbon N. Y.* **162**, 187–194 (2020). <https://doi.org/10.1016/j.carbon.2020.02.032>
43. S. Ke, B. Wang, P. Lu, Plasmonic absorption enhancement in periodic cross-shaped graphene arrays. 2015 IEEE MTT-S Int. Microw. Work. Ser. Adv. Mater. Process. RF THz Appl. IEEE MTT-S IMWS-AMP 2015 - Proc. **23**, 4810–4817 (2015). doi:<https://doi.org/10.1109/IMWS-AMP.2015.7325015>.
44. Y. Avitzour, Y.A. Urzhumov, G. Shvets, Wide-angle infrared absorber based on a negative-index plasmonic metamaterial. *Phys. Rev. B.* **79**, 045131 (2009). <https://doi.org/10.1103/PhysRevB.79.045131>
45. Z.Q. Liu, H.B. Shao, G.Q. Liu, X.S. Liu, H.Q. Zhou, Y. Hu, X.N. Zhang, Z.J. Cai, G. Gu, A 3/20000 Plasmonic nanocavities with multispectral ultra-narrowband absorption for high-quality sensing. *Appl. Phys. Lett.* **104**, 2–6 (2014). <https://doi.org/10.1063/1.4867028>
46. C. Wu, Y. Avitzour, G. Shvets, Ultra-thin wide-angle perfect absorber for infrared frequencies. *Metamaterials Fundam. Appl.* **7029**, 70290W (2008). <https://doi.org/10.1117/12.797208>
47. J. Chen, H. Nie, T. Zha, P. Mao, C. Tang, X. Shen, G.S. Park, Optical magnetic field enhancement by strong coupling in metamaterials. *J. Light. Technol.* **36**, 2791–2795 (2018). <https://doi.org/10.1109/JLT.2018.2822777>
48. W. Wang, F. Yan, S. Tan, H. Zhou, Y. Hou, Ultrasensitive terahertz metamaterial sensor based on vertical split ring resonators. *Photonics Res.* **5**, 571 (2017). <https://doi.org/10.1364/prj.5.000571>
49. M. Pu, C. Hu, M. Wang, C. Huang, Z. Zhao, C. Wang, Q. Feng, X. Luo, Design principles for infrared wide-angle perfect absorber based on plasmonic structure. *Opt. Express.* **19**, 17413 (2011). <https://doi.org/10.1364/OE.19.017413>
50. N. Liu, M. Mesch, T. Weiss, M. Hentschel, H. Giessen, Infrared perfect absorber and its application As plasmonic sensor. *Nano Lett.* **10**, 2342 (2010)
51. W. Zhu, X. Zhao, Metamaterial absorber with dendritic cells at infrared frequencies. *J. Opt. Soc. Am. B.* **26**, 2382 (2009). <https://doi.org/10.1364/josab.26.002382>

**Publisher's Note** Springer Nature remains neutral with regard to jurisdictional claims in published maps and institutional affiliations.